ACS OMEGA

http://pubs.acs.org/journal/acsodf

Article

Chemical, Electrochemical, and Surface Morphological Studies of the Corrosion Behavior of the AZ31 Alloy in Simulated Body Fluid: Effect of NaOH and H_2O_2 Surface Pretreatments on the Corrosion Resistance Property

Husnu Gerengi,* Marina Cabrini, Moses M. Solomon, Ertugrul Kaya, Luca Gritti, and Mehmet Lutfi Yola

Cite This: *ACS Omega* 2022, 7, 26687−26700

Read Online

ACCESS | Metrics & More | Article Recommendations | Supporting Information

ABSTRACT: Magnesium and its alloys have attracted attention for biomedical implant materials in dental and orthopedic applications because of their biodegradability and similar properties to human bones. The very high rate of degradation in the physiological systems is, however, a major setback to their utilization. Chemical modification is one of the approaches adopted to enhance the corrosion resistance property of Mg and its alloys. In this work, NaOH and H_2O_2 were used as a pretreatment procedure to improve the corrosion resistance of the AZ31 Mg alloy in simulated body fluid (SBF). Advanced techniques such as dynamic electrochemical impedance spectroscopy (dynamic-EIS), atomic force microscopy, and optical profilometry were used in addition to the classical mass loss, hydrogen evolution, EIS, and polarization techniques to study the corrosion resistance property of the alloy in SBF for 30 h. Results obtained show that the surface treatment significantly enhanced the corrosion resistance property of the alloy. From dynamic-EIS at 30 h, the charge transfer resistance of the untreated AZ31 Mg alloy is 432.6 Ω cm^2, whereas 822.7 and 2617.3 Ω cm^2 are recorded for NaOH- and H_2O_2-treated surfaces, respectively. H_2O_2 is a better treatment reagent than NaOH. The mechanism of corrosion of both untreated and treated samples in the studied corrosive medium has been discussed.

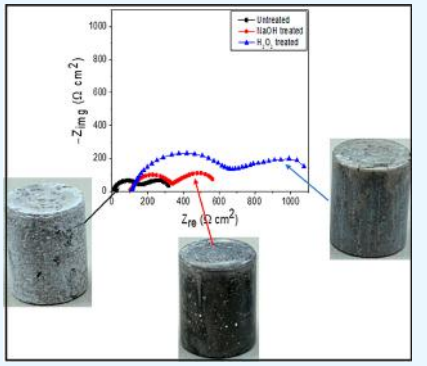

1. INTRODUCTION

Historically, the use of alloys in surgical implants dates back to the 19th century when stainless steel was used to develop the fracture plate.[1,2] Since then, several permanent implants have been developed from metals such as titanium, chromium, vanadium, cobalt, and so forth.[1,2] However, permanent metal implants are challenged by long-term risks of chronic inflammation as the human body always perceives them as foreign bodies. Up to date, the design, material selection, and biocompatibility remain the three critical issues in biomedical implants and devices. The successful development of MAGNEZIX screws from magnesium alloys for application as an implant for fixation in orthopedics, trauma, and sports surgery[3] has, however, raised the hope of overcoming the challenges associated with permanent metal implants.

Magnesium is biocompatible with the human body. A healthy adult requires a daily magnesium intake of 300−400 mg. Magnesium in the body is important for the growth of bone tissues.[4−6] Magnesium ions dissolve easily in body fluid and are nontoxic. Additionally, the density (1.74−2 g/cm^3) and Young's modulus (41−45 GPa) of magnesium are close to the density (1.8−2.1 g/cm^3) and Young's modulus (3−20 GPa) of human body's bone; hence, the stress shielding effect is avoided when using the magnesium implant.[7,8]

Although biodegradability is a desirable characteristic for implants, the rapid degradation rate of pure Mg in body fluid of the pH level 7.4−7.6 and in chloride-rich physiological systems is unacceptable. It is essential that an implant provides sufficient mechanical support to the surrounding tissues until the healing process is completed and should degrade without causing serious inflammatory or immunological response.[4−7]

It is a fact that certain properties of Mg including the corrosion resistance property can be enhanced by alloying Mg with elements such as Al, Zn, Mn, Cr, and so forth.[4,7] Mg−Al alloys, in particular, had been reported to exhibit improved properties than pure Mg.[7] The AZ31 alloy, for instance, which is the most popular Mg−Al alloy is known to have ultralow density, good energy absorption, and excellent damping

Received: May 13, 2022
Accepted: July 7, 2022
Published: July 20, 2022

Downloaded via UNIV DI BERGAMO on August 30, 2022 at 08:21:56 (UTC).
See https://pubs.acs.org/sharingguidelines for options on how to legitimately share published articles.

© 2022 The Authors. Published by American Chemical Society

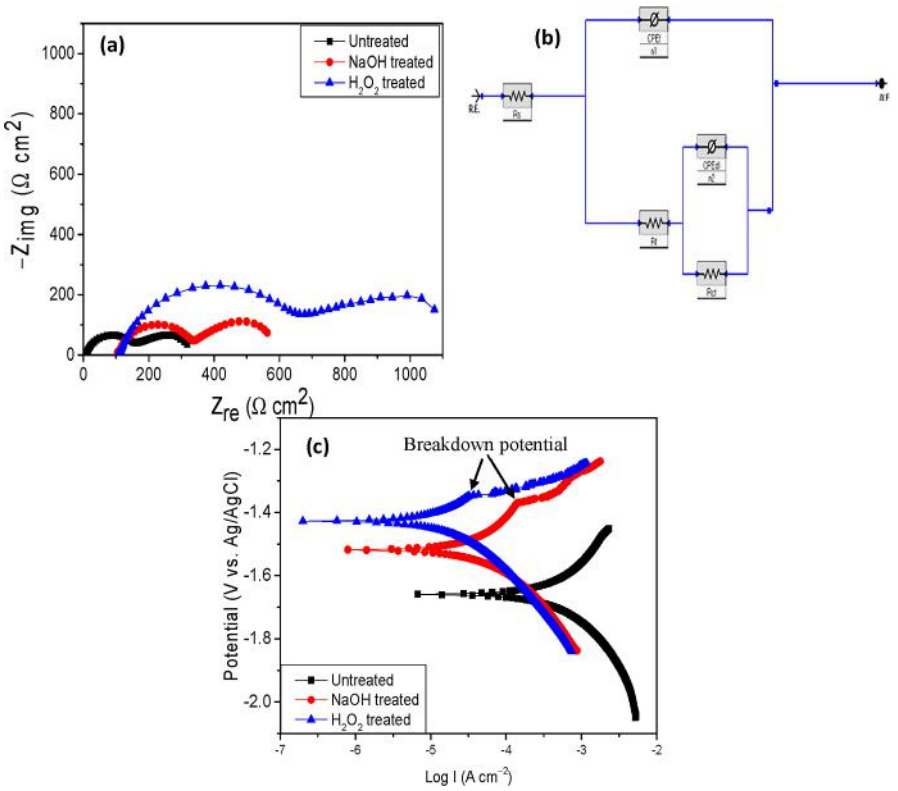

Figure 1. Electrochemical behavior of the untreated and treated AZ31 Mg alloy in SBF—(a) impedance characteristic in Nyquist representation, (b) electrical equivalent circuit used for impedance modeling, and (c) polarization characteristic.

performance in comparison to the pure Mg.[7] Unfortunately, the corrosion resistance property of Mg alloys in body fluid and physiological systems is still unacceptable.[4−7]

Several approaches, which can be broadly grouped into two, (i) surface modification (such as chemical treatments, coatings, anodization, *etc.*[6,9,10]) and (ii) composition and/or microstructure modification,[2,4,7] have been developed to control the degradation rate of metals in the biological systems. The chemical treatments and coatings are directed toward the inducement of hydroxyapatite (HA) on the metal surface.[6,9,10] It was reported that chemical treatment of titanium and its alloys using NaOH and H_2O_2 induced the formation of bone-like apatite *in vitro* and *in vivo* and that the apatite layer did not exhibit the problems associated with the apatite produced *via* coatings by other techniques such as plasma spray. For instance, Wang *et al.*[10] modified the surface of pure titanium specimens with NaOH and H_2O_2/HCl. The bioactivity of the treated metal in simulated body fluid (SBF) was evaluated. It was found that H_2O_2/HCl treatment produced an anatase titania gel layer, while NaOH treatment produced a sodium titanate gel layer on the specimen surface. The gel layers induced bone-like apatite during staking in SBF. Shukla and Balasubramaniam[9] reported the formation of one additional layer on CP Ti and two additional layers on Ti−6Al−4V and Ti−13Nb−13Zr alloys after alkaline surface treatment and immersion in Hank's solution. The improved bioactivity and corrosion behavior of some Mg alloys in SBF occasioned by the surface treatment with NaOH and H_2O_2 had also been demonstrated.[6] More so, the chemical modification technique is simple, cost-effective, and flexible.[6,9,10] Although significant research studies have been undertaken to understand the influence of chemical treatment using NaOH and H_2O_2 on the bioactivity and electrochemical behavior of titanium and its alloys in body fluid solution,[6,9,10] such work is rather scanty for magnesium and its alloys. In Sasikumar *et al.*[6] studies, it was found that bone-like HA can be formed and grown on the surface of Mg alloys through NaOH and H_2O_2 surface treatment. However, the classical weight loss and electrochemical techniques were used in the investigation. It is important to use advanced techniques in this kind of research.

In this present work, we attempt to provide greater insights into the effect of NaOH and H_2O_2 surface treatment on the bioactivity and corrosion property of the AZ31 alloy in SBF. Advanced techniques, namely, dynamic electrochemical impedance spectroscopy (dynamic-EIS), atomic force microscopy, and optical profilometry, are employed. The extent of stability of the protective HA layers formed as a result of the surface treatment is also monitored. The dynamic-EIS technique, which is more reliable than the conventional EIS method due to its ability to accurately and continuously track changes in a dynamic environment, is used to track the changes in the alloy surface properties in the SBF for as long as 30 h. The conventional EIS requires three strict conditions, namely, linearity, causality, and a stationary state to be met.[11]

2. RESULTS AND DISCUSSION

2.1. Corrosion Behavior of the Untreated and Treated AZ31 Mg Alloy in SBF. *2.1.1. Electrochemical Impedance Spectroscopy and Potentiodynamic Polarization Studies.* The impedance characteristics of the untreated and treated AZ31 Mg alloy in SBF are illustrated in Figure 1. The measurements were carried out after 110,000 s of free corrosion (Figure S1). The open circuit potential (E_{oc}) of the untreated alloy is in the region of −1.83 to −1.65 V *versus* Ag/

https://doi.org/10.1021/acsomega.2c02998
ACS Omega 2022, 7, 26687−26700

Table 1. Electrochemical Parameters of the Untreated and Treated AZ31 Mg Alloy in SBF at 25 °C Obtained From (a) EIS and (b) PDP Techniques

	(a) EIS							
alloy sample	R_s (Ω cm^2)	R_f (Ω cm^2)	CPE_f (μF cm^{-2})	n_f	R_{ct} (Ω cm^2)	CPE_{dl} (μF cm^{-2})	n_{dl}	R_t (Ω cm^2)
untreated AZ31	8.9	151.4	0.463	0.87	182.2	0.281	0.78	333.6
NaOH-treated AZ31	10.6	235.5	0.230	0.86	276.0	0.239	0.83	511.5
H_2O_2-treated AZ31	10.9	526.3	0.146	0.78	566.7	0.205	0.83	1093.0
	(b) PDP							
alloy sample	E_{corr} (V vs.Ag/AgCl)		I_{corr} (μA cm^{-2})		βa (mV/dec)	βc (mV/dec)	corrosion rate (mpy)	
untreated AZ31	1.66		2010.0		905.2	565.1	3347.8	
NaOH-treated AZ31	1.52		404.0		647.7	304.3	672.9	
H_2O_2-treated AZ31	1.43		126.0		466.7	278.8	209.9	

AgCl and is in conformity with the values reported in the literature.[5,6,12] The treated samples exhibit nobler potentials (−1.69 to −1.53 V *vs* Ag/AgCl for NaOH-treated and −1.52 to −1.42 V *vs* Ag/AgCl for H_2O_2-treated) than the untreated sample implying less susceptibility to corrosion probably due to the presence of a protective film on the treated surfaces.[6]

As mentioned earlier, the surface treatment involves the soaking of the alloy samples in NaOH or H_2O_2 solution followed by heat treatment. The soaking process, according to a previous report, produced the $Mg(OH)_2$ layer on the surface.[6] Because of the strong oxidizing power of H_2O_2, a denser $Mg(OH)_2$ layer is expected. During heat treatment, $Mg(OH)_2$ dehydrates and MgO is formed.[13] It had been reported[14] that the corrosion product formed when Mg and its alloys are exposed to SBF is a mixture of $Mg(OH)_2$, MgO, and HA. HA can slow down alloy degradation under physiological conditions and has also been reported to enhance cell growth, proliferation, and healing around bone implants.[14] Presently, HA is used as a biomedical material and possesses excellent biocompatibility and bioactivity due to its chemical and structural similarities to bone and tooth minerals.[15,16] Ascencio *et al.*[13] reported that the top-most corrosion product layer on the WE43 Mg alloy exposed to modified SBF was an amorphous $Mg(OH)_2$ and carbonated apatite mixture. Although MgO, $Mg(OH)_2$, and HA have protective ability,[17] the growth of $Mg(OH)_2$ is rather controlled by a dissolution−precipitation mechanism.[18] The homeostasis of the dissolution−precipitation mechanism is destabilized by chloride ions in SBF such that $Mg(OH)_2$ is transformed into $MgCl_2$.[6,13,17]

The Nyquist graphs in Figure 1 are similar and indicate that the surface treatment did not change the corrosion mechanism of the alloy in SBF. The graphs exhibit two circular loops at the high and medium frequencies corresponding to the two-time constants and denote two different interfacial processes. The capacitive loop at high frequency represents the resistance to the charge transfer process across the corrosion product and/or protective film layer,[19] while the loop at the medium frequency describes the diffusion processes of ions such as Mg^{2+} through the surface layer.[19] There is an enlargement of the capacitive loops of the treated samples relative to the untreated, with the H_2O_2-treated loop being the largest. This observation, which conforms with the E_{oc} results (Figure S1), suggests a thicker or a more rigid protective film on the H_2O_2-treated surface than on the NaOH-treated surface.

It is worth pointing out the disparity in the characteristics of our obtained impedance (Figure 1) and those reported in the corrosion literature.[5−7,20] Our impedance exhibits two-time constant behavior, whereas most Mg impedances in SBF are three-time constants,[5−7,20] that is, capacitive loops at high and medium frequencies and an inductive loop in the low-frequency region. This disparity is due to the differences in the time of impedance measurements. As it is known, the inductive loop in the low-frequency region is related to the breakdown of the surface film or relaxation of adsorbed species such as $Mg(OH)_2$.[5−7] As mentioned earlier, the corrosion product formed when Mg and its alloys are immersed in SBF is in layers: the outer porous $Mg(OH)_2$ and the carbonated apatite mixture layer and the inner MgO layer.[7,13] McIntyre and Chen[21] reported that the MgO layer could be up to 2.2 nm thick after 10 s and would increase logarithmically with time. Our E_{oc} results (Figure S1) reveal that the outer $Mg(OH)_2$ layer on the treated alloy surfaces collapsed at about 30,000 s of immersion in the studied medium. Such a breaking point is not observed in the E_{oc}−time graph of the untreated sample (Figure S1). This suggests the collapsing of the preformed $Mg(OH)_2$ layer rather than the accumulated corrosion product layers. After the breaking point, the graphs show a steady increase in open circuit potential, suggesting the continuous thickening of the corrosion product layer. The implication is that the corrosion product layer was intact as at the time (30 h) of measurement; hence, the observed two-time constant behavior. Wen *et al.*[7] noticed that the impedance of an AZ31 Mg alloy in modified SBF showed three-time constants at 1−6 h of measurements but became two-time constants at 24 h of measurement. Xin *et al.*[22] reported only one capacitive loop for the AZ91 Mg alloy in a nonbuffered SBF at 36 h of immersion and attributed it to the rupturing of the protective layer and the occurrence of pitting corrosion.

The fitting of the impedance response (Figure 1) was carried out using a two-time constant electrical equivalent circuit (EC) shown in Figure 1b. The impedance response, as expected from a solid electrode with varying degrees of surface roughness and heterogeneities, exhibits a nonideal capacitive behavior. For this reason, a constant phase element (CPE) was introduced in the EC to obtain a better experimental data fit. The modeled EC describes the alloy surface as follow: R_s denotes the solution resistance between the working and the reference electrodes; R_{ct} and CPE_{dl} represent the charge transfer resistance and the electrochemical characteristic of the double layer capacitance at the electrode/electrolyte interface, respectively; and R_f and CPE_f represent the resistance to the diffusion of Mg^{2+} and other possible ions through the outer film layer.[13] The impedance of a CPE (Ω cm^2) is defined using eq 1[13]

$$Z_{CPE} = Q^{-1}(jw)^{-n} \quad (1)$$

https://doi.org/10.1021/acsomega.2c02998
ACS Omega 2022, 7, 26687−26700

Table 2. Dynamic Electrochemical Parameters of the Untreated and Treated AZ31 Mg Alloy Obtained After 30 h of Immersion in SBF at 25 °C

alloy sample	R_s (Ω cm^2)	R_f (Ω cm^2)	CPE$_f$ (μF cm^{-2})	n_f	R_{ct} (Ω cm^2)	CPE$_{dl}$ (μF cm^{-2})	n_{dl}	R_t (Ω cm^2)
untreated AZ31	20.3	163.6	0.346	0.91	269.0	0.356	0.70	432.6
NaOH-treated AZ31	87.6	245.7	0.740	0.91	577.0	0.687	1.00	822.7
H_2O_2-treated AZ31	86.0	1921.0	0.201	0.92	696.3	1.411	0.67	2617.3

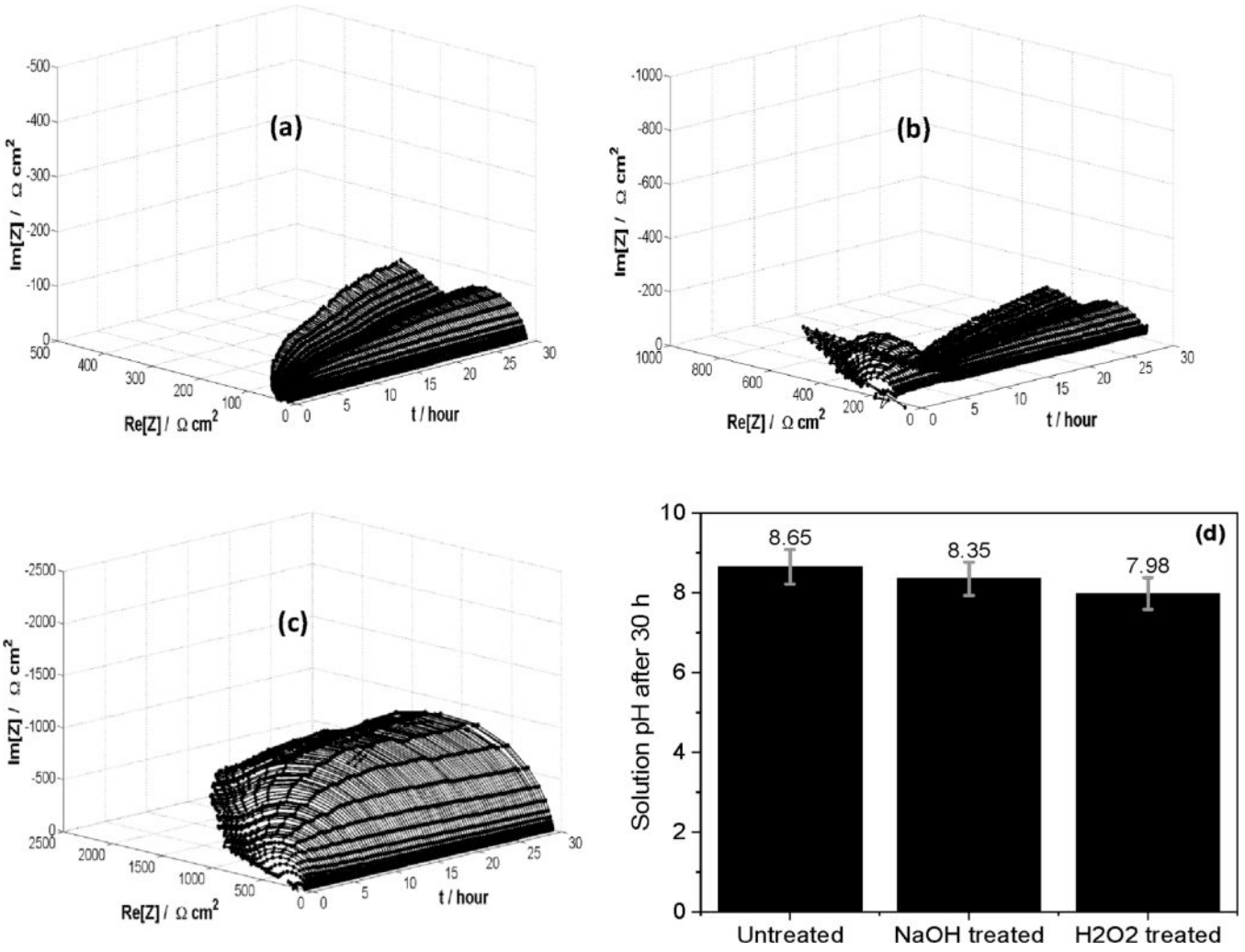

Figure 2. Dynamic electrochemical behavior of the (a) untreated, (b) NaOH-treated, and (c) H_2O_2-treated AZ31 Mg alloy in SBF. (d) pH of SBF after Mg alloy immersion for 30 h at 25 °C.

where Q is a constant and has the unit Ω^{-1} cm^{-2} s^n, n is a dimensionless constant and is in the range $-1 \leq n \leq 1$, j is the imaginary number and is expressed as $j = (-1)^{0.5}$, and w is the angular velocity given as $w = 2\pi f$ (f is the frequency). The values derived from the fitting of the experimental data are given in Table 1a. The total resistance (R_t) also listed in Table 2 is the sum of R_f and R_{ct}. At 30 h of impedance measurements, the R_t of the untreated alloy is 333.6 Ω cm^2, while that of NaOH- and H_2O_2-treated alloy samples is 511.5 and 1093.0 Ω cm^2, respectively. Clearly, the H_2O_2-treated alloy surface possesses an excellent corrosion resistance property than the NaOH-treated surface. It is interesting to note the smaller CPE$_f$ and CPE$_{dl}$ values obtained for the treated surfaces relative to the untreated surface. This parameter provides information on the characteristics of the surface film.[23] The smaller CPE$_f$ and CPE$_{dl}$ values for the treated surfaces compared to the untreated surface are indicative of a more compact and thicker film on the treated surfaces.[23]

The polarization curves obtained for the untreated and treated AZ31 Mg alloy samples after 30 h of immersion in SBF at 25 °C are shown in Figure 1c. The polarization parameters derived from the analysis of the curves are also listed in Table 1b. Compared to the polarization curve of the untreated sample, the corrosion potential (E_{corr}) of the treated samples is nobler and the anodic and cathodic corrosion current densities are remarkably reduced (Figure 1c). The E_{corr} of the untreated sample is −1.66 V *versus* Ag/AgCl but −1.52 V *versus* Ag/AgCl and −1.43 V *versus* Ag/AgCl for NaOH- and H_2O_2-treated samples, respectively (Table 1b). The corrosion current density (I_{corr}) of the treated samples (404.0 μA cm^{-2} for NaOH-treated and 126.0 μA cm^{-2} for H_2O_2-treated sample) is appreciably lower than that of the untreated sample (2010.0 μA cm^{-2}). Consequently, a corrosion rate of 3347.8 mpy of the

https://doi.org/10.1021/acsomega.2c02998
ACS Omega 2022, 7, 26687−26700

untreated alloy decreased to 672.9 and 209.9 mpy upon treatment with NaOH and H_2O_2, respectively. Worthy to note in Table 1b is the fact that the βa and βc values are considerably smaller for the treated samples relative to the untreated, meaning that the surface treatment affected both the anodic and cathodic corrosion reactions. All these observations are indicative of the significant improvement of the corrosion resistance property of the AZ31 Mg alloy in SBF occasioned by the chemical surface modification, especially H_2O_2 surface modification. Also worthy of note is the passivation phenomenon in the anodic arms of the treated sample polarization curves (Figure 1c). In the referred curves, a breakdown potential is observed at about −1.42 V *versus* Ag/AgCl (marked in Figure 1c), which is in agreement with the behavior noted in the E_{oc} *versus* time graphs (Figure S1) and could be associated with the breakdown of the $Mg(OH)_2$ layer.[24] Beyond the breakdown potential, a passivating tendency is observed. Similar observation has been reported in the literature and was interpreted to indicate the presence of the oxide film on the surface.[24,25]

2.1.2. Dynamic-EIS Studies. The dynamic-EIS is designed to overcome the challenges associated with the classical EIS technique.[26] Because corrosion is dynamic in nature, achieving a steady-state condition as required by the classical EIS is practically impossible and defaulting always have some effects on the EIS results.[27] The dynamic-EIS is an application of short-time Fourier transform coupled with the multi-sinusoid perturbation signal that allows the tracking of changes on surfaces in nonstationary systems with time, potential, current, and temperature.[28,29] A detailed information on the dynamic-EIS technique can be found elsewhere.[28,29] In Figure 2 is presented the dynamic-EIS spectra of the (a) untreated, (b) NaOH-treated, and (c) H_2O_2-treated AZ31 Mg alloy in SBF as tracked continuously for 30 h at 25 °C.

The spectra reveal that the chemistry and/or composition of the surface film changes with immersion time. In the first 10 h of immersion, the impedance exhibits three-time constant behavior (very clear in Figure 2b), agreeing with the report of Wen *et al.*[7] and denoting the processes of charge transfer, diffusion, and relaxation of adsorbed species.[19] Beyond this time, the impedance characteristic switched to two-time constants, in perfect agreement with the EIS results (Figure 1). The beneficial effect of surface modification is clearly seen in the figure. For instance, the Re/Z/in Figure 2a terminates at about 200 Ω cm^2, whereas it terminates at about 800 and 2000 Ω cm^2 in Figure 2b,c, respectively. To interpret the results quantitatively, the equivalent circuit in Figure 1c was used for analysis and the parameters obtained are presented in Table 3. Clearly, the chemical modification, particularly H_2O_2 surface modification, significantly boosted the corrosion resistance property of the alloy. The R_t value for the untreated surface is 432.0 Ω cm^2, while that of the NaOH- and H_2O_2-treated surfaces is 822.7 and 2617.3 Ω cm^2, respectively. The NaOH and H_2O_2 surface treatment enhanced the alloy surface corrosion resistance by 47.42 and 83.47%, respectively. It is also obvious in Figure 2d that the treated alloy surfaces possess better corrosion resistance in SBF than the untreated AZ31 alloy. While the pH of the SBF containing the untreated sample increased from the initial value of 7.4 to 8.65, the pH of the SBF solution containing NaOH- and H_2O_2-treated samples increased to 8.35 and 7.98, respectively. According to Ascencio *et al.*,[13] the pH increase is due to the production of OH^- species as a result of corrosion processes and the release of CO_2 to the atmosphere ($H_2CO_3 \leftrightarrow CO_2 + H_2O$). The lowest pH value in SBF solution containing the H_2O_2-treated sample therefore suggests the lowest corrosion processes and the most favorable environment for cell growth on the surface.[6,30]

Table 3. Calculated Values of Weight Loss and the Corrosion Rate of the Untreated and Treated AZ31 Mg Alloy Immersed in SBF at 25 °C for 1.25 days (30 h)

		corrosion rate (mpy)		
alloy sample	weight loss (g)	weight loss	PDP	hydrogen evolution
untreated AZ31	0.055	3362.573	3347.775	3726.013
NaOH-treated AZ31	0.011	672.515	672.886	698.628
H_2O_2-treated AZ31	0.0033	201.754	209.861	232.876

A comparison of the results from the classical EIS technique to that of the dynamic-EIS technique (Table 2) reveals a marked difference. For instance, the R_t value obtained from the classical EIS for the untreated, NaOH-, and H_2O_2-treated surfaces is 333.6, 511.5, and 1093.0 Ω cm^2, respectively, but 432.0, 822.7, and 2617.3 Ω cm^2 from the dynamic-EIS. As mentioned earlier, the classical EIS requires three strict conditions of linearity, causality, and stationary state to be met for accurate measurement.[31]

To further gain insights into the corrosion process and to investigate how the immersion duration affected the AZ31 Mg alloy corrosion mechanisms, the R_f, R_{ct}, and R_t were plotted as a function of time (Figure 3). An initial gradual increase in R_f, R_{ct}, and R_t with time is observed in treated surfaces. For the NaOH-treated surface, the R_f, R_{ct}, and R_t increased and reached a value of about 532, 453, and 985 Ω cm^2, respectively, at around 20,000 s. For the H_2O_2-treated surface, the R_f, R_{ct}, and R_t increased, reaching a value of about 985, 1580, and 2539 Ω cm^2, respectively, at around 60,000 s. The untreated surface seems to maintain an increase in open potential throughout the measurement duration. This initial increase in R_f, R_{ct}, and R_t can be related to the formation of the surface layers that offer protection to the surface.[13] After the initial increase, a decrease in R_f, R_{ct}, and R_t with time is observed and is related to an increase in exposure of the underlying substrate surface to the corrosive solution as a result of the rupturing of the surface layer, probably the preformed $Mg(OH)_2$ layer.[13] In the case of the NaOH surface, the decrease in R_f, R_{ct}, and R_t is seen to be very sharp relative to that of H_2O_2-treated surface, suggesting than H_2O_2 treatment produced a more compact and denser surface film than NaOH treatment, that is, H_2O_2 is a better surface treatment agent than NaOH. However, it is observed that the decline in the total corrosion resistance of the surfaces is largely caused by a decrease in R_f (Figure 3a). This seems to confirm the earlier assertion that the observed decrease in the surface charge transfer resistance was due to the deterioration of the outer $Mg(OH)_2$ layer. Hence, the protection observed thereafter as evidenced by the higher value of R_f, R_{ct}, and R_t is from the inner preformed MgO and the newly formed $Mg(OH)_2$ and apatite layers.

2.1.3. Mass Loss and Hydrogen Evolution Studies. The mass loss technique was also used to study the rate of degradation of AZ31 Mg alloy samples in SBF. The physical appearance of the AZ31 Mg alloy samples after immersion in the SBF for 30 h (1.25 days) at 25 °C is shown in Figure S2.

https://doi.org/10.1021/acsomega.2c02998
ACS Omega 2022, 7, 26687−26700

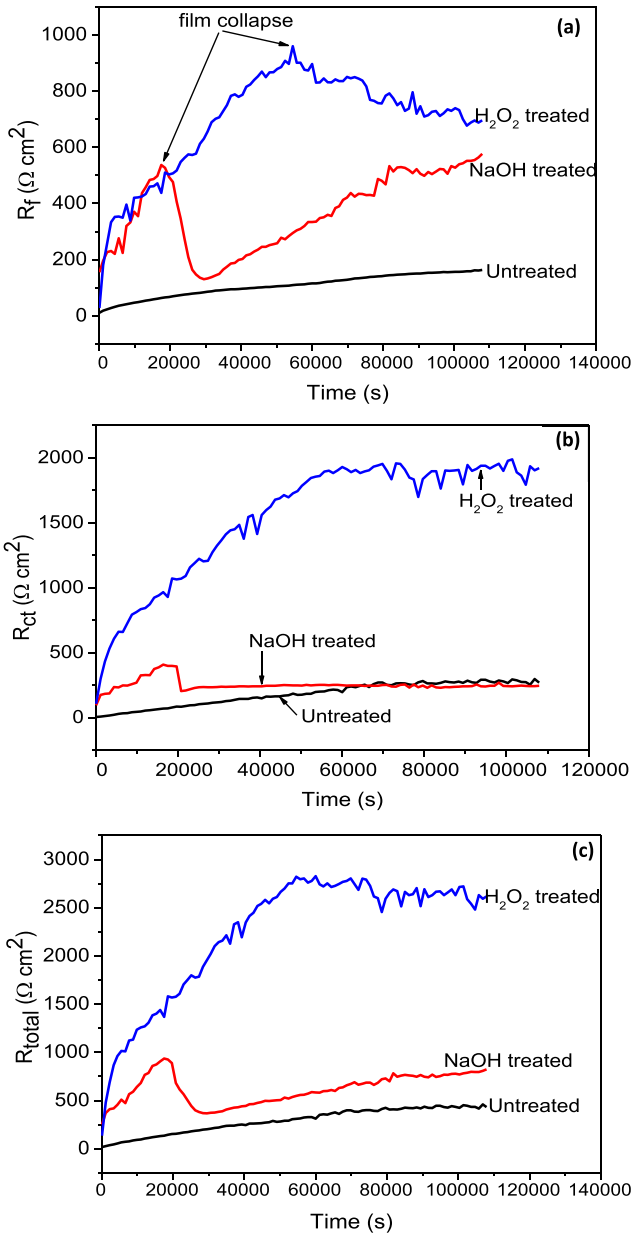

Figure 3. Variation of (a) film resistance, (b) charge transfer resistance, and (c) total resistances of the untreated and treated AZ31 Mg alloy immersed in SBF at 25 °C for 30 h.

The surface of the untreated sample (Figure S2(1)) is covered with the "chalk-like" corrosion product identified by authors[32] to be the insoluble Ca-rich oxide. This product can be problematic in the body if it builds up too rapidly.[32] In addition, a varying degree of pitting is seen on the surface of the untreated sample. In the treated surfaces (Figure S2(2 and 3)), less Ca-rich oxide and pitting are spotted, inferring slower corrosion processes than the untreated sample. The weight loss (g), the degradation rate (mpy), and the rate of corrosion resistance enhancement by the surface treatment (%) calculated from the mass loss experiments are given in Table 3. The untreated sample corroded by 917.07 mpy, while the NaOH- and H_2O_2-treated samples corroded by 427.96 and 61.14 mpy, respectively. NaOH surface treatment enhanced the alloy corrosion resistance by 26.7%, while the boost *via* H_2O_2 treatment is 78%.

Magnesium in the aqueous environment degrades according to eq 2.[5,22] The volume of hydrogen gas liberated from the reaction can be related to the rate of dissolution.[5,22] The hydrogen evolution technique is reliable, easy to implement, and not prone to errors because the corrosion products do not influence the relationship between hydrogen evolution and magnesium dissolution.[22] Figure S3 shows the evolution of hydrogen gas with time for untreated, NaOH-treated, and H_2O_2-treated AZ31 Mg alloy upon immersion in SBF at 25 °C. For the untreated sample, a steady hydrogen gas evolution is observed with immersion time. As stated earlier, the evolution of hydrogen gas due to the corrosion process in physiological systems is too fast to be dealt with by the host tissues;[22] the reason modification is a necessity. Clearly, the surface treatment with NaOH and H_2O_2 brought about a substantial decrease in the volume of hydrogen gas evolved in the SBF.

$$Mg + 2H_2O \rightarrow Mg(OH)_2 + H_2\uparrow \quad (2)$$

The corrosion rates (mpy) obtained from the PDP, weight loss, and hydrogen evolution techniques are comparable (Table 3).

2.2. Characteristics of Untreated and Treated AZ31 Mg Alloy-Corroded Surfaces. *2.2.1. XRD Studies.* Figure 4 shows the X-ray diffraction (XRD) patterns of the corrosion products on the (a) untreated, (b) NaOH-treated, and (c) H_2O_2-treated AZ31 Mg alloy surface after 3, 6, 24, and 30 h of immersion in SBF at 25 °C. The corrosion product, as revealed by the XRD results, is a mixture of $Mg(OH)_2$, MgO, and apatite in agreement with reports in the literature.[6,13,16] Inspection of the figure reveals the influence of the immersion time on the $Mg(OH)_2$, MgO, and apatite layers. In both the untreated and treated surfaces, a decrease in the diffraction band intensity of the apatite peak at about $2\theta = 38°$ with immersion time is observed, suggesting an increase in the thickness of the corrosion layer with time.[13,16] It is however observed that the diffraction band intensity in Figure 4b,c is stronger than that in Figure 4a, agreeing with the experimental results that the surface treatment improved the corrosion resistance property (Figures 1 and 2). It means that the untreated alloy seriously corroded in the SBF, and the heaps of corrosion products (see. Figure 6) affected the diffraction intensity. Similar argument can be found in the corrosion literature.[19]

2.2.2. SEM and EDAX Studies. The (a) scanning electron microscopy (SEM) and (b) energy-dispersive spectroscopy (EDAX) elemental mapping micrographs of the AZ31 Mg alloy specimen obtained after mechanical abrasion are shown in Figure 5. The EDAX elemental composition is given in Table 4. The EDAX elemental mapping micrographs (Figure 5b) reveal evenly distributed Mg, Al, and Zn on the abraded surface (Figure 5a). The weight percentage of Mg as detected by EDAX (Table 4) is 95.75%. The weight percentage of the alloying elements is 3.16 and 1.09% for Al and Zn, respectively. The alloy sample severely corroded in SBF (Figure 6a), and the Mg content detected decreased to 21.20% (Table 4) due to the covering of the surface by corrosion products (Figure 6a). Two regions are seen on the corroded surface in Figure 6a: the cracked bottom region and the sparingly distributed chalk-like product on the top region. The cracking of the bottom region may be due to the dehydration of the corrosion product layer caused by the vacuum atmosphere created during SEM analysis.[13] The cracked inner layer corresponds to the magnesium oxide/hydroxide layer[33] formed due to the

https://doi.org/10.1021/acsomega.2c02998
ACS Omega 2022, 7, 26687−26700

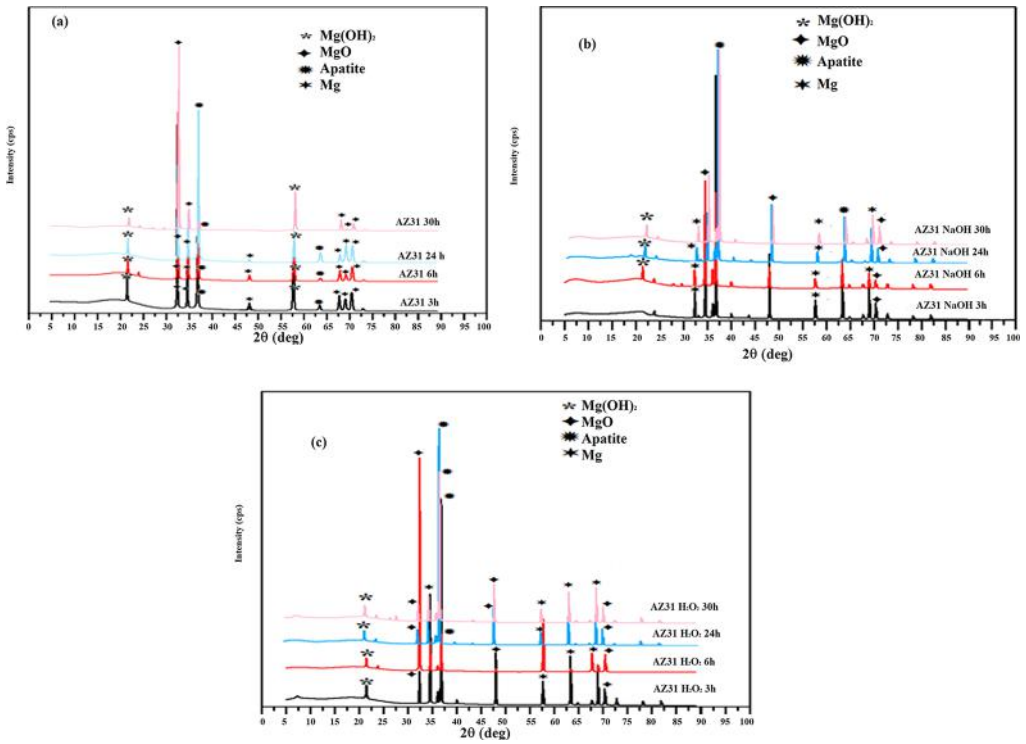

Figure 4. XRD diffraction patterns of the (a) untreated, (b) NaOH-treated, and (c) H_2O_2-treated AZ31 Mg alloy after 3, 6, 24, and 30 h of immersion in SBF at 25 °C.

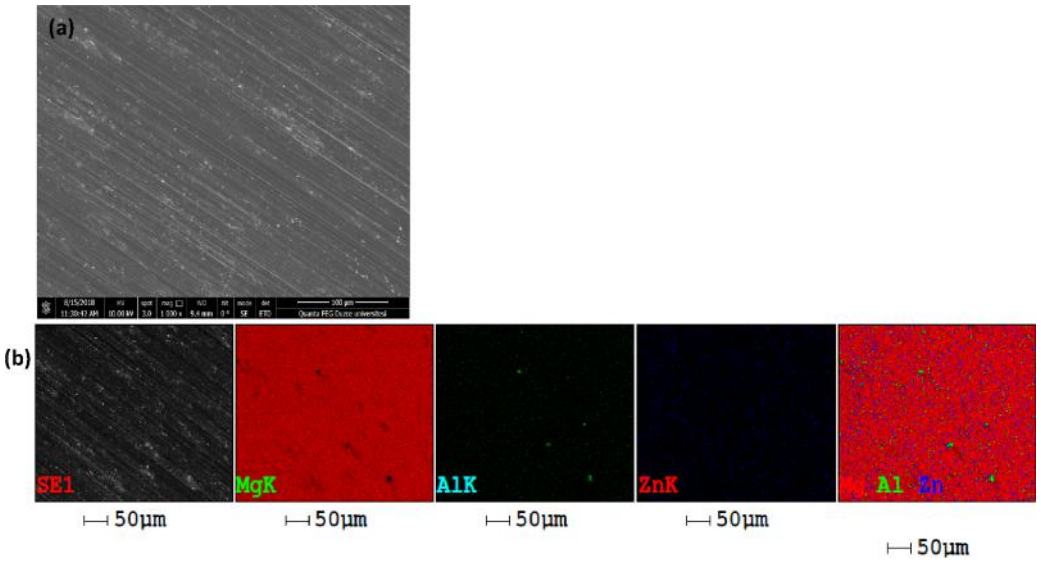

Figure 5. (a) SEM and (b) EDAX elemental mapping micrographs of the AZ31 Mg alloy after mechanical abrasion.

Table 4. EDAX Results for the AZ31 Mg Alloy under Various Conditions

	wt. %											
AZ31 Mg alloy	C	O	Al	Mg	P	Zn	Mn	Na	Cl	K	Ca	N
after mechanical abrasion			3.16	95.75		1.09						
untreated AZ31 Mg alloy after immersion in SBF for 30 h at 25 °C	3.75	48.54	4.83	21.20	10.40	1.55	0.37	1.54	0.72	0.28	6.82	
NaOH-treated AZ31 Mg alloy after immersion in SBF for 30 h at 25 °C.	3.35	39.28	5.78	24.68	13.28	1.48	0.54	1.12	0.14	0.28	9.09	0.98
H_2O_2-treated AZ31 Mg alloy after immersion in SBF for 30 h at 25 °C.	9.11	39.16	5.60	24.03	8.93	0.88	0.70	2.87	3.58	0.40	4.75	

https://doi.org/10.1021/acsomega.2c02998
ACS Omega 2022, 7, 26687−26700

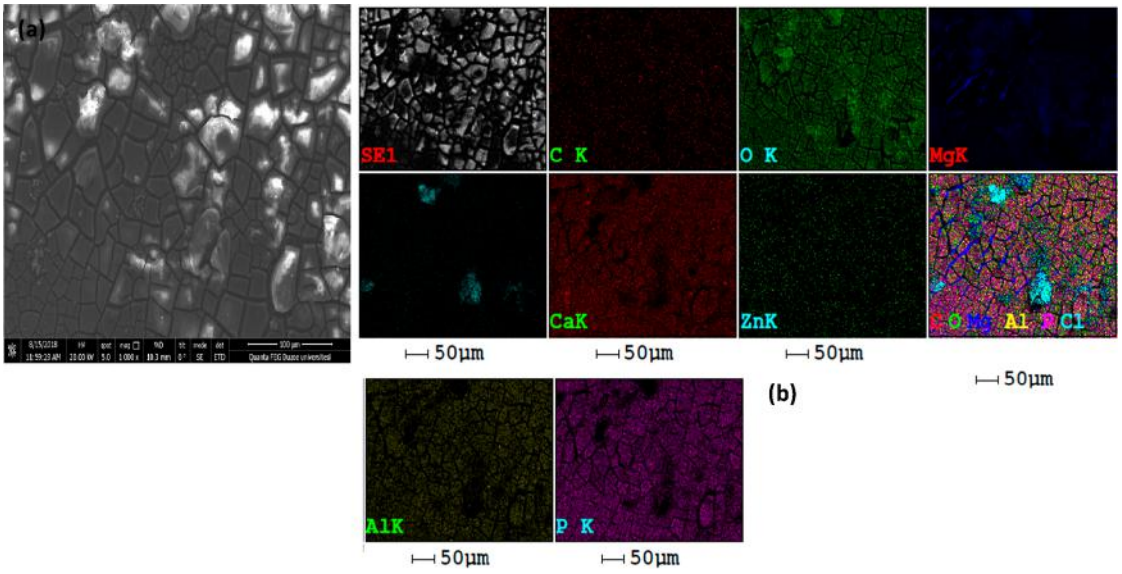

Figure 6. (a) SEM and (b) EDAX elemental mapping micrographs of the untreated AZ31 Mg alloy after immersion in SBF for 30 h at 25 °C.

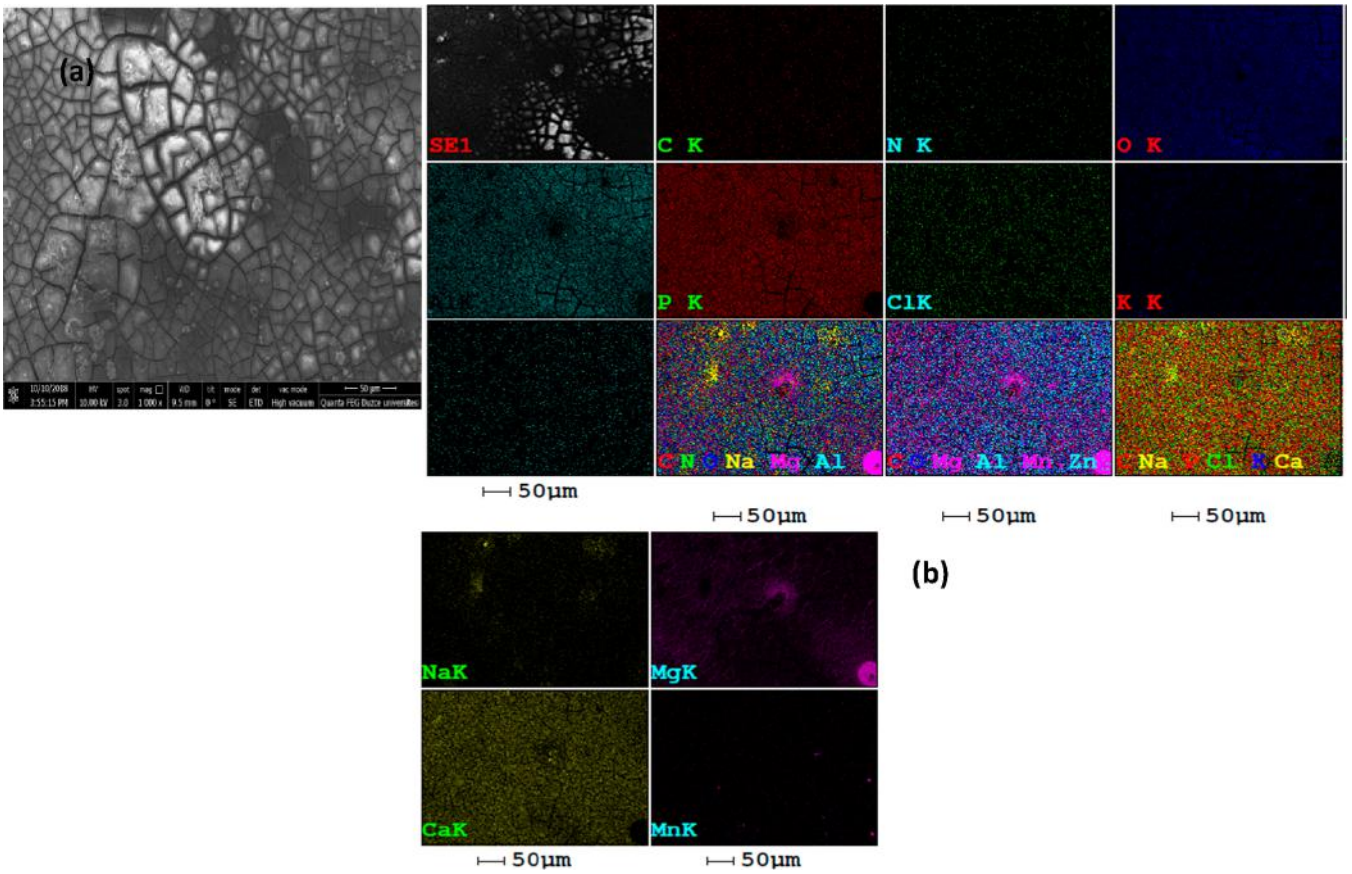

Figure 7. (a) SEM and (b) EDAX elemental mapping micrographs of the NaOH-treated AZ31 Mg alloy after immersion in SBF for 30 h at 25 °C.

preferential attack on the α-Mg matrix.[13] The chalk-like topmost layer, which is very obvious in the EDAX elemental mapping-combined micrograph (Figure 6b), is assigned to precipitated phosphate and carbonate.[13,33] The presence of C, O, and P in Table 4 provides experimental evidence to the claim that the corrosion product is a mixture of oxide, hydroxide, phosphate, and carbonate.

The SEM and EDAX elemental mapping micrographs of NaOH- and H_2O_2-treated AZ31 Mg alloy samples after immersion in SBF for 30 h at 25 °C are given in Figures 7 and 8, respectively. The surfaces in Figures 7a and 8a, just like the one in Figure 6a, exhibit cracked morphology. Such intergranular cracks are common in an alkaline environment.[34] However, the heat treatment could as well contribute to the cracking of these surfaces. In contrast, the surfaces in Figures

https://doi.org/10.1021/acsomega.2c02998
ACS Omega 2022, 7, 26687−26700

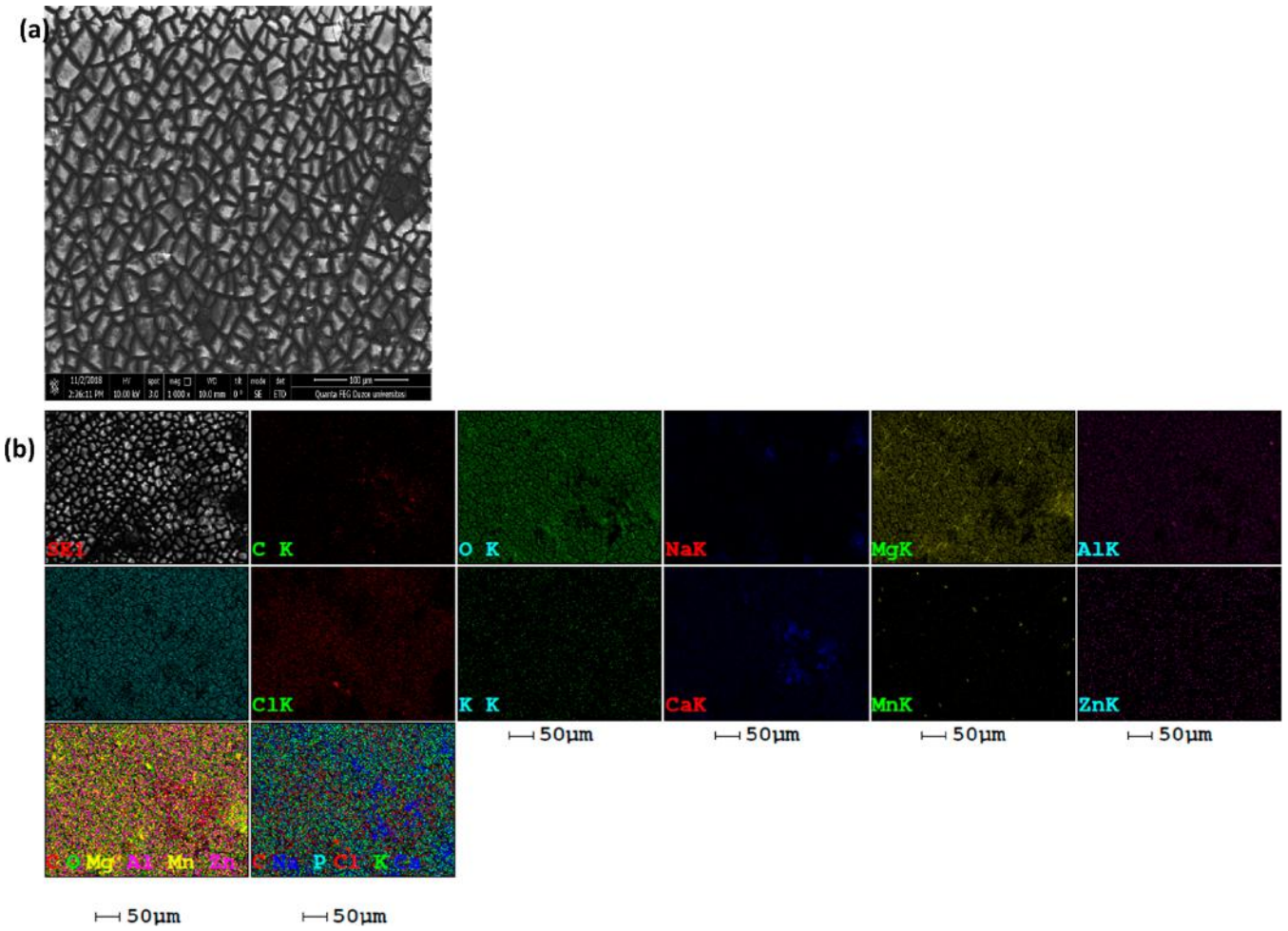

Figure 8. (a) SEM and (b) EDAX elemental mapping micrographs of the H_2O_2-treated AZ31 Mg alloy after immersion in SBF for 30 h at 25 °C.

7a and 8a appear more compact (especially, the surface in Figure 8a) than the surface in Figure 6a. The EDAX elemental mapping micrographs (Figures 7b and 8b) clearly show that the elements were more uniformly distributed on the surfaces in Figures 7a and 8a than on the surface in Figure 6a. These observations confirm the experimental results (Tables 2 and 3) that the surface treatment benefited the corrosion resistance property of the alloy in the studied corrosive medium. There is a slight decrease in O content, in Table 4 (39.28% for the NaOH-treated surface and 39.16% for the H_2O_2-treated surface relative to 48.54% for the untreated corroded surface), which is probably due to the covering of the oxide layer by the apatite layer.

2.2.3. OP and AFM Studies. The surface roughness and topography of the untreated and treated AZ31 Mg alloy sample surfaces after immersion in SBF for 30 h at 25 °C were investigated by optical profilometry and atomic force microscopy (AFM) techniques. In Figure 9 is presented the 3D optical profilometry and 2D AFM images of the alloy samples and the associated roughness parameters. The degree of surface roughness can be used to explain the extent of damage to a surface.[35] The optical profilometry (OP) images (Figure 9) reveal that the alloy samples (both untreated and treated) suffered a certain degree of pitting corrosion in the exposed corrosive medium. The untreated sample suffered the severest pitting corrosion with the pit depth measuring up to 3.755 μm (Figure 9a) followed by the NaOH-treated surface (pit depth = 1.806 μm) (Figure 9b). The H_2O_2-treated surface suffered the least pitting corrosion, and the measured pit depth is 0.544 μm (Figure 9c).

The AFM results (Figure 9d–f) are in good agreement with the OP results (Figure 9a–c). The roughest surface is the untreated alloy with an average value of profile deviation from the mean line (R_a) of 20,192–30,691 μm and an average peak to valley height (R_z) of 77,912–89,907 μm (Figure 9c). The surface roughness of the NaOH- and H_2O_2-treated surfaces relative to the untreated surface remarkably reduced. The R_a and R_z values reduced to 5049–8763 μm and 25,354–33,645 μm, respectively, in the case of NaOH-treated surface. For the H_2O_2-treated surface, the R_a and R_z values reduced to 4504–5760 and 19,160–19,943 μm, respectively. These results corroborate other results (Figures 1, 2, 6, 7, and 8) and confirm the beneficial effect of the NaOH and H_2O_2 surface treatments on the corrosion resistance property of the AZ31 Mg alloy in SBF.

2.3. Corrosion Mechanism of the Untreated and Treated AZ31 Mg Alloy in SBF. Based on the results obtained from this investigation, the mechanism of corrosion of the AZ31 Mg alloy in SBF is proposed. **Stage 1** (surface treatment): The soaking of the alloy samples in NaOH or H_2O_2 for 1 h produced the $Mg(OH)_2$ layer on the alloy surface. Heat treatment at 250 °C for 4 h caused $Mg(OH)_2$ film shrinkage due to dehydration (as evidenced in the cracked surface morphology in Figures 6 and 7); MgO is also formed in

https://doi.org/10.1021/acsomega.2c02998
ACS Omega 2022, 7, 26687–26700

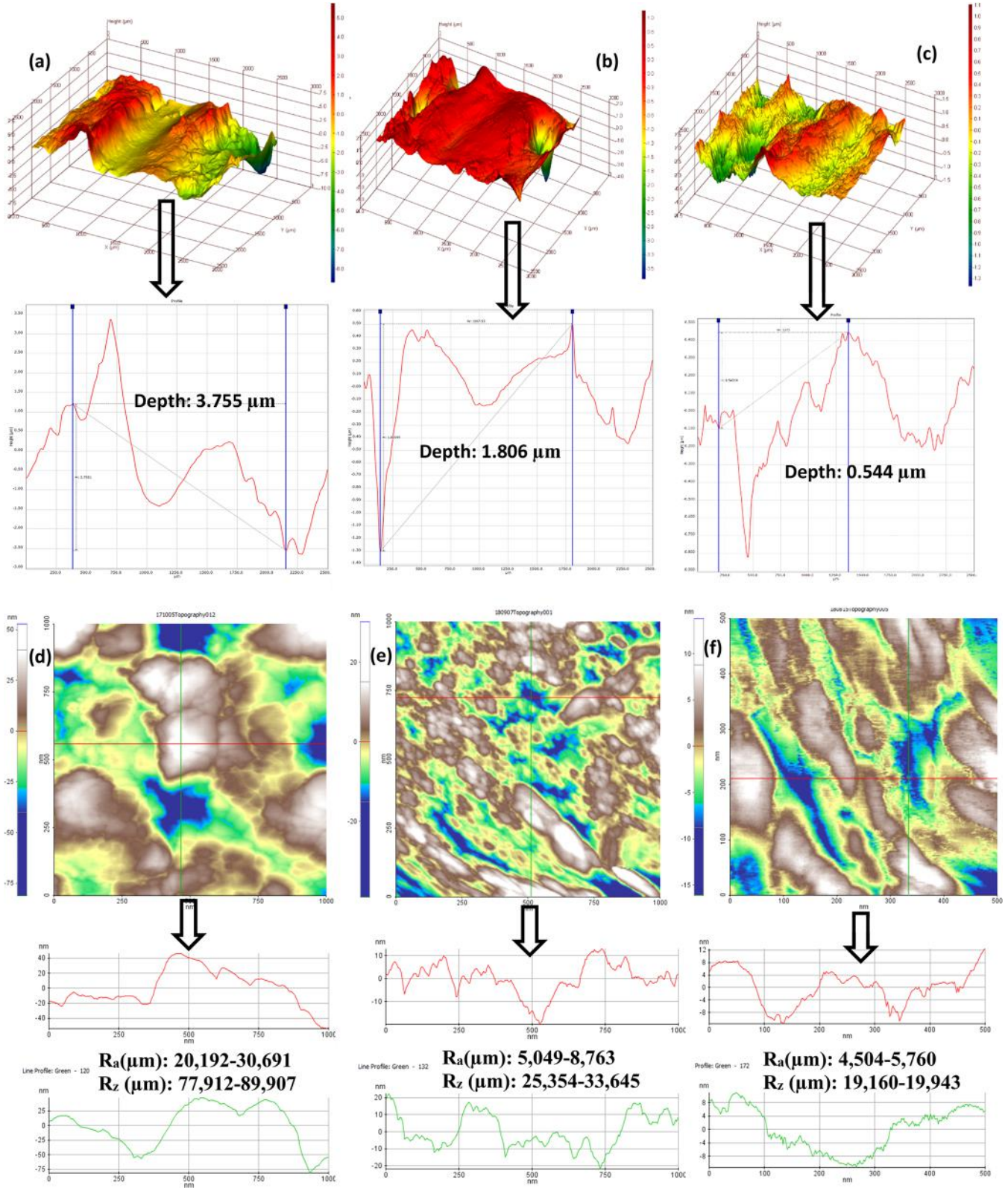

Figure 9. Optical profilometry and AFM micrograph of the (a,d) untreated, (b,e) NaOH-treated, and (c,f) H_2O_2-treated AZ31 Mg alloy after immersion in SBF for 30 h at 25 °C.

the process according to eq 3.[13] The treated sample surfaces thus have MgO beneath the $Mg(OH)_2$ layer.

$$Mg(OH)_2 \leftrightarrow MgO + H_2O \quad (3)$$

Stage 2 (immersion in SBF): The electrochemical oxidation of the α-Mg matrix and the corresponding electrochemical hydrogen reduction reactions occur according to eqs 4 and 5.[36]

$$2Mg \rightarrow 2Mg^{2+} + 2e^{-} \text{ (anodic reaction)} \quad (4)$$

https://doi.org/10.1021/acsomega.2c02998
ACS Omega 2022, 7, 26687−26700

$$2H_2O + 2e^- \rightarrow H_2 + 2OH^- \text{ (cathodic reaction)} \quad (5)$$

The initial rapid corrosion rate causes an increase in the concentration of Mg^{2+} and OH^- ions as evidenced in the increase in the solution pH (Figure 2d). The Mg^{2+} and OH^- ions generated in eqs 4 and 5 combined and formed the corrosion product according to eq 6.

$$Mg^{2+} + 2OH^- \rightarrow Mg(OH)_2 \quad (6)$$

Also, the HCO_3^- and HPO_4^{2-} in the SBF react with some of the OH^- ions generated from the cathodic reaction to induce the precipitation of the insoluble carbonates and phosphates in the corrosion product layer (Figures 6, 7, and 8) according to the eqs 7 and 8:[37]

$$Mg^{2+} \text{ (or } Ca^{2+}) + OH^- + HPO_4^{2-} + (n-1)H_2O \rightarrow Mg_x(\text{or Ca})(PO_4)_y \bullet nH_2O \quad (7)$$

$$Mg^{2+} \text{ (or } Ca^{2+}) + OH^- + HCO_3^- + (n-1)H_2O \rightarrow Mg_x(\text{or Ca})(CO_3)_y \bullet nH_2O \quad (8)$$

These products, as evidenced in Figure 3, possess protective properties and thicken over time. The high corrosion resistance property observed for the treated surfaces (Figures 2, 3, and 4) is the summation of the protective property of the preformed MgO and $Mg(OH)_2$ and the accumulated $Mg(OH)_2$ and apatite produced from the metal dissolution in SBF.

Stage 3 (breaking point): In the SBF, Cl^- ions infiltrated the preformed $Mg(OH)_2$ layer converting some to the soluble $MgCl_2$ (eq 9)[5,13]

$$Mg(OH)_2 + 2Cl^- \rightarrow Mg^{2+} + 2Cl^- + 2OH^- \quad (9)$$

This breakdown is obvious in Figure 3. The collapse of the preformed $Mg(OH)_2$ layer expose the MgO inner layer, and it induced the passivation seen in the polarization curves (Figure 1d). At the same time, $Mg(OH)_2$ and apatite layers formed from the corrosion process continue to grow as noted in Figure 3. According to Ascencio *et al.*,[13] the formation of a corrosion layer with an increasing thickness and protective ability would cause a decrease in water molecules accessing the substrate/corrosion layer interface that would in turn cause $Mg(OH)_2$ dehydration.

3. CONCLUSIONS

The corrosion behavior of the AZ31 Mg alloy in SBF up to 30 h has been studied. The effect of chemical surface treatment using NaOH and H_2O_2 as the treatment reagents has also been examined. Based on the results obtained, the following conclusions are drawn:

i. AZ31 Mg alloy corrodes considerably in SBF.
ii. NaOH and H_2O_2 surface treatment promote the formation of MgO and $Mg(OH)_2$ layers on the Mg surface. The layers exhibit corrosion protective property.
iii. H_2O_2 is a better surface treatment reagent than NaOH.
iv. In SBF, MgO, $Mg(OH)_2$, and apatite are the corrosion products on the AZ31 Mg alloy surface.
v. The NaOH and H_2O_2 preformed $Mg(OH)_2$ layer collapsed at about 20,000 and 60,000 s, respectively, upon immersion in SBF. However, surface protection is restored by the overlying MgO layer and the newly formed apatite and $Mg(OH)_2$ layers.
vi. The treated AZ31 Mg alloy sample suffers minimal pitting corrosion relative to the untreated sample.

4. EXPERIMENTAL SECTION

4.1. Sample Preparation and Electrolyte. The AZ31 Mg alloy supplied by Goodfellow Cambridge Limited, England was used in this investigation. The chemical composition (wt %) of the alloy is Al (2.89), Zn (0.92), Mn (0.05), Si (0.01), Cu (0.002), Ni (0.001), Fe (0.004), and balance Mg.[12] For weight loss experiments, the sample dimension was 20 × 25 × 0.5 mm^3. For electrochemical experiments, the flat AZ31 Mg alloy sheet was mechanically cut into working samples of 1 cm^2 as the surface area. In order to provide the electrical conductivity, the samples were carefully soldered into a copper wire and insulated to obtain 0.76 cm^2 as the exposed surface area. Prior to surface treatment, the exposed surface area of the samples was wet-abraded using abrasive paper up to 2000-grit. Thereafter, the abraded samples were fine-polished with diamond paste, ultrasonically cleaned in ethanol, rinsed in acetone in order to remove abrasion and polishing debris, and dried in warm air of about 40 °C.

The SBF has the following composition: $CaCl_2$ (0.292 g mL^{-1}), KCl (0.225 g mL^{-1}), $K_2HPO_4 \cdot 3H_2O$ (0.231 g mL^{-1}), $MgCl_2 \cdot 6H_2O$ (0.311 g mL^{-1}), NaCl (8.035 g mL^{-1}), $NaHCO_3$ (0.355 g mL^{-1}), and Na_2SO_4 (0.072 g mL^{-1}). Tris-hydroxymethyl aminomethane and HCl were used to adjust the electrolyte pH to 7.4. The quantitative information on the ions in SBF and the organic part of human blood plasma can be found in our previous publication.[6]

4.2. Surface Treatment. The procedure reported by Sasikumar *et al.*[6] was followed. First, the native oxide layer on the AZ31 Mg alloy surface was removed by washing the samples in a HCl/H_2O (ratio 1:4 in volume) mixture for 2 min at 60 °C. Thereafter, the samples were ultrasonically cleaned in deionized water for about 10 min and then dried at normal temperature.

For the NaOH surface treatment, the prepared AZ31 Mg alloy samples were immersed in 20 mL of 10 M NaOH maintained at 60 °C for 24 h. The samples were retrieved, gently washed in deionized water, and dried at 40 °C for 24 h. The dried specimens were afterward heat-treated in an electric furnace at 250 °C for 4 h and cooled to room temperature in the furnace. Finally, the specimens were ultrasonically cleaned to remove the loosely attached particles over the surface of the specimens.

For the H_2O_2 surface treatment, the prepared AZ31 Mg samples were immersed in 20 mL of 4.5 M H_2O_2 placed in an oven at 80 °C for 1 h. The samples were thereafter subjected to similar treatments as described for the NaOH surface modification approach.

4.3. Mass Loss and Hydrogen Evolution Experiments. Three 200 mL capacity glass bottles marked as untreated AZ31, NaOH-treated AZ31, and H_2O_2-treated AZ31 were filled with 150 mL of SBF. The respective alloy samples (*i.e.*, untreated AZ31, NaOH-treated AZ31, and H_2O_2-treated AZ31) were suspended freely with the help of a thread in the bottles. They were placed in a digital thermostatic water bath maintained at 25 °C for 30 h. The samples were retrieved and dipped in aqueous solution of chromium trioxide/silver nitrate/barium nitrate as recommended by the ASTM G1-03

https://doi.org/10.1021/acsomega.2c02998
ACS Omega 2022, 7, 26687−26700

standard[38] for 1 min. The exact composition of the pickling solution is withheld for proprietary reasons. Thereafter, the samples were washed in running water and distilled water, cleaned with acetone, and dried with warm air. The mass of the dried samples was measured, and the mass loss was calculated as the difference between the initial and the final masses of the coupons. The corrosion rate (ν) in mpy and the percentage corrosion resistance enhancement (η) by the surface treatment were calculated using eqs 10 and 11, respectively,

$$\mathrm{v} = \frac{K \times W}{A \times T \times D} \tag{10}$$

$$\eta = \frac{v_0 - v_1}{v_0} \times 100 \tag{11}$$

where $K = 3.45 \times 10^6$, W = mass loss (g), A = exposed area (cm^2), T = immersion time (h), D = density in g/cm^3, v_0 = corrosion rate of the untreated alloy, and v_1 = corrosion rate of the treated alloy.

The rate of corrosion of the untreated and treated AZ31 Mg alloy in SBF was also studied by monitoring the volume of hydrogen gas liberated at 2 h interval for 30 h. The diagram of the experimental setup for the hydrogen evolution can be found elsewhere.[22] From the hydrogen evolution results, the corrosion current density (j_{corr}) was first calculated and then used to calculate the corrosion rate (V_{corr}) given in Table 3 using eqs 12 and 13, respectively.[39,40] The V_{corr} values were thereafter converted from mm/y to mpy.

$$j_{corr}\ (\mathrm{A\ cm^{-2}}) = \frac{2pVF}{tART} \tag{12}$$

$$V_{corr}\ (\mathrm{mm\ /y}) = \frac{j_{corr} K E_W}{dA} \tag{13}$$

where p is the pressure in Pascal, V is the volume of hydrogen gas (cm^3) evolved in time t (s), F is Faraday's constant, A is the surface area of the sample in cm^2, R is the molar gas constant, T is the temperature in Kelvin, K is equal to 3272 and is the conversion factor, E_W is the equivalent weight, and d is the density in g/cm^3.

4.4. pH Measurements. Before and after dynamic-EIS measurements, the pH of the SBF + alloy sample system was recorded using an ISOLAB hand-type pH meter.

4.5. Electrochemical Experiments. EIS and potentiodynamic polarization (PDP) experiments were performed using a conventional Gamry potentiostat/galvanostat/ZRA (Reference 600) instrument, while a National Instruments Measurement Ltd. PCI-4461digital analogue card and potentiostat/galvanostat were deployed for dynamic-EIS experiments.[41] The two instruments are triple-electrode systems. In our case, a saturated Ag/AgCl electrode was used as the reference electrode, a platinum mesh was used as the counter electrode, and the AZ31 Mg alloy samples were used as the working electrode. Prior to EIS experiments, the open circuit potential (OCP) was monitored for 3600 s. Impedance measurements were carried out at frequency ranging from 100 kHz to 0.1 Hz, and the amplitude signal utilized was 10 mV peak-to-peak. Impedance analysis was performed using ZsimpWin 3.21 software. For PDP experiments, the working electrode was scanned at −300 to +300 mV interval with reference to corrosion potential using a constant sweep rate of 1 mV/s. Analysis of the polarization curves was carried out using the Gamry Echem Analyst program. For dynamic-EIS, the sampling frequency was 12.8 kHz, the perturbation signal was in the range of 4.5 kHz−300 mHz, and the measurement was carried out for 30 h. Detailed information on how the National Instruments Measurement Ltd. PCI-4461digital analogue card works can be found in our previous publications.[42−45] Each experiment was repeated three times, and the average values are presented in this work.

4.6. Characterization of Corroded Surfaces. The X-ray powder diffraction (XRD) pattern of both the untreated and treated alloy surfaces was recorded at 3, 6, 24, and 30 h of immersion in SBF at 25 °C using a Röntgen PW3040/60X'Pert Pro X-ray diffractometer with Ni-filtered Cu-Kα radiation (k = 1.5405 A°) in the range of 5−90° with a scanning rate of 1 deg min^{-1}. The analysis of the XRD data was achieved with X'Pert HighScore Plus PW3212 software. The surface morphology of the tested samples in SBF after 30 h of immersion was examined using a scanning electron microscope Quanta FEG 250 model that is coupled to an EDAX probe (accelerator voltage 20 keV) for composition determination. The EDAX was also used to map the distribution of each element on the alloy surface. AFM and OP studies were carried out using the Park System X-100E AFM model and optical profilometer (Phaseview ZeeScope), respectively.

■ ASSOCIATED CONTENT

Supporting Information

The Supporting Information is available free of charge at https://pubs.acs.org/doi/10.1021/acsomega.2c02998.

Variation of open circuit potential with time for the untreated and treated AZ31 Mg alloy immersed in SBF for 30 h at 25 °C; physical appearance of the untreated, NaOH-treated, and H_2O_2-treated AZ31 Mg alloy after immersion in SBF for 30 h at 25 °C; and graph showing the evolution of hydrogen gas with time for the untreated, NaOH-treated, and H_2O_2-treated AZ31 Mg alloy upon immersion in SBF at 25 °C (PDF)

■ AUTHOR INFORMATION

Corresponding Author

Husnu Gerengi − *Corrosion Research Laboratory, Department of Mechanical Engineering, Faculty of Engineering, Duzce University, Duzce 81620, Turkey; Department of Engineering and Applied Sciences, University of Bergamo, Bergamo 24044, Italy;* orcid.org/0000-0002-9663-4264; Email: husnugerengi@gmail.com

Authors

Marina Cabrini − *Department of Engineering and Applied Sciences, University of Bergamo, Bergamo 24044, Italy*

Moses M. Solomon − *Department of Chemistry, College of Science and Technology, Covenant University, Ota 112104, Nigeria*

Ertugrul Kaya − *Corrosion Research Laboratory, Department of Mechanical Engineering, Faculty of Engineering, Duzce University, Duzce 81620, Turkey;* orcid.org/0000-0003-1579-6411

Luca Gritti − *Department of Engineering and Applied Sciences, University of Bergamo, Bergamo 24044, Italy*

Mehmet Lutfi Yola − *Department of Nutrition and Dietetics, Faculty of Health Sciences, Hasan Kalyoncu University,*

https://doi.org/10.1021/acsomega.2c02998
ACS Omega 2022, 7, 26687−26700

Gaziantep 27010, Turkey; orcid.org/0000-0001-7424-3425

Complete contact information is available at: https://pubs.acs.org/10.1021/acsomega.2c02998

Notes

The authors declare no competing financial interest.

■ ACKNOWLEDGMENTS

H.G. expresses his appreciation to The Scientific and Technological Research Council of Turkey (TUBITAK) for financial support under the TUBITAK 2219-International Postdoctoral Research Fellowship (program project number: 1059B191900111).

■ REFERENCES

(1) Park, J. B.; Park, J. B. Metallic Implant Materials. In *Biomaterials Science and Engineering*; Springer US, 1984; pp 193−233.
(2) Balamurugan, A.; Rajeswari, S.; Balossier, G.; Rebelo, A. H. S.; Ferreira, J. M. F. Corrosion Aspects of Metallic Implants—An Overview. *Mater. Corros.* **2008**, *59*, 855−869.
(3) Biber, R.; Pauser, J.; Geßlein, M.; Bail, H. J. Magnesium-Based Absorbable Metal Screws for Intra-Articular Fracture Fixation. *Case Rep Orthop.* **2016**, *2016*, 9673174.
(4) Liu, M.; Wang, J.; Zhu, S.; Zhang, Y.; Sun, Y.; Wang, L.; Guan, S. Corrosion Fatigue of the Extruded Mg−Zn−Y−Nd Alloy in Simulated Body Fluid. *J. Magnesium Alloys* **2020**, *8*, 231−240.
(5) Song, Y.; Shan, D.; Chen, R.; Zhang, F.; Han, E. H. Biodegradable Behaviors of AZ31 Magnesium Alloy in Simulated Body Fluid. *Mater. Sci. Eng., C* **2009**, *29*, 1039−1045.
(6) Sasikumar, Y.; Solomon, M. M.; Olasunkanmi, L. O.; Ebenso, E. E. Effect of Surface Treatment on the Bioactivity and Electrochemical Behavior of Magnesium Alloys in Simulated Body Fluid. *Mater. Corros.* **2017**, *68*, 776−790.
(7) Wen, Z.; Wu, C.; Dai, C.; Yang, F. Corrosion Behaviors of Mg and Its Alloys with Different Al Contents in a Modified Simulated Body Fluid. *J. Alloys Compd.* **2009**, *488*, 392−399.
(8) Song, G. Control of Biodegradation of Biocompatable Magnesium Alloys. *Corrosion Sci.* **2007**, *49*, 1696−1701.
(9) Shukla, A. K.; Balasubramaniam, R. Effect of Surface Treatment on Electrochemical Behavior of CP Ti, Ti-6Al-4V and Ti-13Nb-13Zr Alloys in Simulated Human Body Fluid. *Corros. Sci.* **2006**, *48*, 1696−1720.
(10) Wang, X.-X.; Hayakawa, S.; Tsuru, K.; Osaka, A. A Comparative Study of in Vitro Apatite Deposition on Heat-, H2O2-, and NaOH-treated Titanium Surfaces. *J. Biomed. Mater. Res.* **2001**, *54*, 172−178.
(11) Gamry Accurate Electrochemical Impedance Spectroscopy EIS. https://www.gamry.com/application-notes/EIS/accurate-eis/(accessed 28 Jun 2020).
(12) Sahu, P. K.; Das, J.; Chen, G.; Liu, Q.; Pal, S.; Zeng, S.; Shi, Q. Friction Stir Selective Alloying of Different Al% Particulate Reinforced to AZ31 Mg for Enhanced Mechanical and Metallurgical Properties. *Mater. Sci. Eng., A* **2020**, *774*, 138889.
(13) Ascencio, M.; Pekguleryuz, M.; Omanovic, S. An Investigation of the Corrosion Mechanisms of WE43 Mg Alloy in a Modified Simulated Body Fluid Solution: The Influence of Immersion Time. *Corros. Sci.* **2014**, *87*, 489−503.
(14) Bornapour, M.; Muja, N.; Shum-Tim, D.; Cerruti, M.; Pekguleryuz, M. Biocompatibility and Biodegradability of Mg-Sr Alloys: The Formation of Sr-Substituted Hydroxyapatite. *Acta Biomater.* **2013**, *9*, 5319−5330.
(15) Denissen, H. W.; de Groot, K.; Makkes, P. C.; van den Hooff, A.; Klopper, P. J. Tissue Response to Dense Apatite Implants in Rats. *J. Biomed. Mater. Res.* **1980**, *14*, 713−721.
(16) Wen, C.; Guan, S.; Peng, L.; Ren, C.; Wang, X.; Hu, Z. Characterization and Degradation Behavior of AZ31 Alloy Surface Modified by Bone-like Hydroxyapatite for Implant Applications. *Appl. Surf. Sci.* **2009**, *255*, 6433−6438.
(17) Jamesh, M. I.; Wu, G.; Zhao, Y.; Jin, W.; McKenzie, D. R.; Bilek, M. M. M.; Chu, P. K. Effects of Zirconium and Nitrogen Plasma Immersion Ion Implantation on the Electrochemical Corrosion Behavior of Mg-Y-RE Alloy in Simulated Body Fluid and Cell Culture Medium. *Corros. Sci.* **2014**, *86*, 239−251.
(18) Nordlien, J. H.; Ono, S.; Masuko, N.; Nisancioglu, K. A Tem Investigation of Naturally Formed Oxide Films on Pure Magnesium. *Corros. Sci.* **1997**, *39*, 1397−1414.
(19) Frignani, A.; Grassi, V.; Zanotto, F.; Zucchi, F. Inhibition of AZ31 Mg Alloy Corrosion by Anionic Surfactants. *Corros. Sci.* **2012**, *63*, 29−39.
(20) Pokharel, D. B.; Liping, W.; Dong, J.; Wei, X.; Etim, I.-I. N.; Subedi, D. B.; Umoh, A. J.; Ke, W. Effect of D-Fructose on the in-Vitro Corrosion Behavior of AZ31 Magnesium Alloy in Simulated Body Fluid. *J. Mater. Sci. Technol.* **2020**, *66*, 202−212.
(21) Mcintyre, N. S.; Chen, C. Role of Impurities on Mg Surfaces under Ambient Exposure Conditions. *Corros. Sci.* **1998**, *40*, 1697−1709.
(22) Xin, Y.; Liu, C.; Zhang, X.; Tang, G.; Tian, X.; Chu, P. K. Corrosion Behavior of Biomedical AZ91 Magnesium Alloy in Simulated Body Fluids. *J. Mater. Res.* **2007**, *22*, 2004−2011.
(23) Gerengi, H.; Sen, N.; Uygur, I.; Solomon, M. M. M. Corrosion Response of Ultra-High Strength Steels Used for Automotive Applications. *Mater. Res. Express* **2019**, *6*, 0865a6.
(24) Jiang, L.; Xu, F.; Xu, Z.; Chen, Y.; Zhou, X.; Wei, G.; Ge, H. Biodegradation of AZ31 and WE43 Magnesium Alloys in Simulated Body Fluid. *Int. J. Electrochem. Sci.* **2015**, *10*, 10422−10432.
(25) Song, Y.; Han, E. H.; Shan, D.; Yim, C. D.; You, B. S. The Effect of Zn Concentration on the Corrosion Behavior of Mg-XZn Alloys. *Corros. Sci.* **2012**, *65*, 322−330.
(26) Slepski, P.; Gerengi, H.; Gece, G.; Kaya, E.; Rizvi, M.; Szociński, M. Electrochemical Evaluation of Sustainable Corrosion Inhibitors via Dynamic Electrochemical Impedance Spectroscopy. *ACS Symp. Ser.* **2021**, *1403*, 61−85.
(27) Gerengi, H. The Use of Dynamic Electrochemical Impedance Spectroscopy in Corrosion Inhibitor Studies. *Prot. Met. Phys. Chem. Surf.* **20182018**, *54*, 536−540.
(28) Darowicki, K.; Orlikowski, J.; Lentka, G. Instantaneous Impedance Spectra of a Non-Stationary Model Electrical System. *J. Electroanal. Chem.* **2000**, *486*, 106−110.
(29) Darowicki, K. Theoretical Description of the Measuring Method of Instantaneous Impedance Spectra. *J. Electroanal. Chem.* **2000**, *486*, 101−105.
(30) Geng, F.; Tan, L. L.; Jin, X. X.; Yang, J. Y.; Yang, K. The Preparation, Cytocompatibility, and in Vitro Biodegradation Study of Pure β-TCP on Magnesium. *J. Mater. Sci. Mater. Med.* **2009**, *20*, 1149−1157.
(31) Lasia, A. *Electrochemical Impedance Spectroscopy and Its Applications*; Springer: United States of America, New York, 2014.
(32) Kirkland, N. T.; Lespagnol, J.; Birbilis, N.; Staiger, M. P. A Survey of Bio-Corrosion Rates of Magnesium Alloys. *Corros. Sci.* **2010**, *52*, 287−291 Pergamon February.
(33) Liu, Y.; Curioni, M.; Liu, Z. Correlation between Electrochemical Impedance Measurements and Corrosion Rates of Mg-1Ca Alloy in Simulated Body Fluid. *Electrochim. Acta* **2018**, *264*, 101−108.
(34) Jiang, G.; Xu, D.; Guo, S.; Liu, L.; Hao, B.; Wang, M. Corrosion Behavior and Mechanisms of Al2O3 and Mo Coated Zircaloy-4 in High-Temperature Lithiated Water. *Corros. Sci.* **2022**, *201*, 110270.
(35) Farhadian, A.; Rahimi, A.; Safaei, N.; Shaabani, A.; Abdouss, M.; Alavi, A. A Theoretical and Experimental Study of Castor Oil-Based Inhibitor for Corrosion Inhibition of Mild Steel in Acidic Medium at Elevated Temperatures. *Corros. Sci.* **2020**, *175*, 108871.
(36) Esmaily, M.; Svensson, J. E.; Fajardo, S.; Birbilis, N.; Frankel, G. S.; Virtanen, S.; Arrabal, R.; Thomas, S.; Johansson, L. G. Fundamentals and Advances in Magnesium Alloy Corrosion. *Prog. Mater. Sci* **2017**, *89*, 92−193 Elsevier Ltd August 1.

(37) Xin, Y.; Hu, T.; Chu, P. K. Degradation Behaviour of Pure Magnesium in Simulated Body Fluids with Different Concentrations of HCO3-. *Corros. Sci.* **2011**, *53*, 1522−1528.
(38) ASTM *G-90 Standard Practice for Preparing, Cleaning, and Evaluating Corrosion Test Specimens.*
(39) Bosch, J.; Martin, U.; Aperador, W.; Bastidas, J. M.; Ress, J.; Bastidas, D. M. Corrosion Behavior of High-Mn Austenitic Fe−Mn−Al−Cr−C Steels in NaCl and NaOH Solutions. *Materials* **2021**, *14*, 1−17.
(40) Wang, J. B.; Wang, J. M.; Shao, H. B.; Zhang, J. Q.; Cao, C. N. The Corrosion and Electrochemical Behaviour of Pure Aluminium in Alkaline Methanol Solutions. *J. Appl. Electrochem.* **2007**, *37*, 753−758.
(41) Gerengi, H.; Cabrini, M.; Solomon, M. M.; Kaya, E. Understanding the Corrosion Behavior of the AZ91D Alloy in Simulated Body Fluid through the Use of Dynamic EIS. *ACS Omega* **2022**, *7*, 11929−11938.
(42) Yildiz, M.; Gerengi, H.; Solomon, M. M.; Kaya, E.; Umoren, S. A. Influence of 1-Butyl-1-Methylpiperidinium Tetrafluoroborate on St37 Steel Dissolution Behavior in HCl Environment. *Chem. Eng. Commun.* **2018**, *205*, 1−11.
(43) Gerengi, H.; Solomon, M. M.; Umoren, S. A.; Ugras, H. I.; Yildiz, M.; Slepski, P. Improved Performance of 1-Ethyl-3-Methylimidazolium Tetrafluoroborate at Steel/HCl Interface by Iodide Ions. *J. Bio- Tribo-Corros.* **2018**, *4*, 12.
(44) Gerengi, H.; Solomon, M. M.; Kaya, E.; Bagci, F. E.; Abai, E. J. An Evaluation of the Anticorrosion Effect of Ethylene Glycol for AA7075-T6 Alloy in 3.5% NaCl Solution. *Meas.: J. Int. Meas. Confed* **2018**, *116*, 264−272.
(45) Gerengi, H.; Solomon, M. M.; Öztürk, S.; Yıldırım, A.; Gece, G.; Kaya, E. Evaluation of the Corrosion Inhibiting Efficacy of a Newly Synthesized Nitrone against St37 Steel Corrosion in Acidic Medium: Experimental and Theoretical Approaches. *Mater. Sci. Eng., C* **2018**, *93*, 539−553.

Recommended by ACS

Characterization and Biocompatibility of Insoluble Corrosion Products of AZ91 Mg Alloys
Weiwei Wu, Huazhe Yang, *et al.*
SEPTEMBER 06, 2019
ACS OMEGA
READ

Pure Mg–Al Layered Double Hydroxide Film on Magnesium Alloys for Orthopedic Applications
Shi Cheng, Yu Zhang, *et al.*
SEPTEMBER 16, 2021
ACS OMEGA
READ

Smart Functionalization of Ceramic-Coated AZ31 Magnesium Alloy
Beatriz Mingo, Aleksey Yerokhin, *et al.*
JUNE 10, 2020
ACS APPLIED MATERIALS & INTERFACES
READ

Microstructure and Corrosion Characterization of a MgO/Hydroxyapatite Bilayer Coating by Plasma Electrolytic Oxidation Coupled with Flame Spraying...
Marzieh Mardali, Babak Safarbali, *et al.*
SEPTEMBER 18, 2020
ACS OMEGA
READ

Get More Suggestions >

https://doi.org/10.1021/acsomega.2c02998
ACS Omega 2022, 7, 26687−26700